PRAMANA
— journal of
physics

Vol. 61, No. 5
November 2003
pp. 889–899

Lattice quantum chromodynamics: Some topics

RAJIV V GAVAI
Department of Theoretical Physics, Tata Institute of Fundamental Research, Homi Bhabha Road, Mumbai 400 005, India

Abstract. I review some topics in lattice quantum chromodynamics, focusing more on the recent results. These include: (i) the QCD phase diagram in the μ–T plane, (ii) the quark number susceptibilities, and (iii) the screening lengths.

Keywords. Lattice; quantum chromodynamics; quark–gluon plasma; susceptibility.

PACS Nos 11.15.Ha; 12.38.Mh

1. Introduction

Most of us at this QCD workshop are aware of the role of the lattice techniques as the only successful tool to extract non-perturbative physics from the theory. Nevertheless, its first principles and (essentially) parameter-free approach is worth emphasizing again in view of the inevitable comparison one makes with the results from other approaches and models. Thus not only does lattice QCD lead us to the phenomenon of quark confinement and spontaneous breaking of chiral symmetry (or why pion is so light) but it also provides us with a quantitative understanding of the spectrum of hadrons and their other properties. Indeed, any experimental demonstration of a failure of a prediction of lattice QCD, such as the transition to quark–gluon plasma, will be tantamount to one of the best experimental evidence for physics beyond the standard model.

For reasons of both time and interest, I have chosen to limit this review to some selected topics. I will begin with a lightning quick overview of the basic lattice gauge theory and then go on to discuss the recent results on the QCD phase diagram, quark number susceptibility and the screening lengths. A short summary is provided at the end.

2. Basic lattice gauge theory

The quark fields, $\psi(x)$, and the antiquark fields $\bar{\psi}(x)$ are associated with a site $x = (x_1, x_2, x_3, x_4)$ of a four-dimensional hypercubic lattice. The (inverse) lattice spacing a acts as the ultraviolet cut-off. Continuum limit of vanishing a corresponds to removal of the cut-off. As in the case of the continuum field theory, one obtains a lattice gauge theory by demanding invariance of the Lagrangian for free quark–antiquarks (e.g. obtained by a straightforward discretization of the usual Dirac Lagrangian) under any *local* phase rotation of these fields. This can be accomplished by introducing lattice gauge fields

$U_x^\mu \equiv U_\mu(x)$ which are associated with a directed link from the site x to $x+\hat{\mu}a$. A simple gauge invariant quark action thus is,

$$S_F = \sum_{x,\mu=1}^{4} \bar{\psi}(x)\gamma_\mu \frac{U_x^\mu \psi(x+\hat{\mu}a) - U_{x-\hat{\mu}a}^{\mu\dagger}\psi(x-\hat{\mu}a)}{2} + ma \sum_x \bar{\psi}(x)\psi(x), \quad (1)$$

where the gauge transformations are defined by

$$\psi'(x) = V(x)\psi(x), \quad \bar{\psi}'(x) = \bar{\psi}(x)V^\dagger(x), \quad U_x'^\mu = V(x)U_x^\mu V^\dagger(x+\hat{\mu}a) \quad (2)$$

and $U_x^\mu \in SU(3), V(x) \in SU(3)$. From the gauge transformations of the U_x^μ-fields, one can see that the simplest gauge invariant action for these fields is given by

$$S_G = \frac{6}{g^2}\sum_P \left[1 - \frac{1}{3}\text{Re tr } U_p\right]. \quad (3)$$

Here $U_p = U_x^\mu U_{x+\hat{\mu}a}^\nu U_{x+\hat{\nu}a}^{\mu\dagger} U_x^{\nu\dagger}$, called plaquette, is the smallest closed loop of the directed gauge links in the (μ,ν) plane at site x. The sum over P runs over all possible plaquettes P on the lattice. Defining $U_x^\mu = \exp[iga\sum_{b=1}^{8} A_\mu^b(x+a\hat{\mu}/2)T^b]$, where $A_\mu^b(x)$ is the continuum gauge field in bth colour direction and μth space direction, and T^b is the corresponding adjoint matrix for bth colour, one can easily show that in the limit of $a \to 0$, eqs (1) and (3) reduce to the usual continuum quark and gauge actions respectively.

Defining a partition function $\mathscr{Z}$ for these fields, which are complicated versions of the familiar Ising spins,

$$\begin{aligned}\mathscr{Z} &= \int \prod_{x,\hat{\mu}} \mathrm{d}U_\mu(x) \prod_x \mathrm{d}\psi(x)\, \mathrm{d}\bar{\psi}(x) \mathrm{e}^{-S_G - S_F} \\ &= \int \prod_{x,\hat{\mu}} \prod_f \det M(am_s, a\mu) \mathrm{e}^{-S_G}, \end{aligned} \quad (4)$$

where M is the Dirac matrix in x, colour, spin, flavour space for fermions of mass am_s and $a\mu$ is the chemical potential (in lattice units). One can compute quantum expectation values of any physical observable Θ, which may contain fermion propagators of mass m_ψ, as averages with respect to the $\mathscr{Z}$ above. Thus, masses of physical particles are obtained from the exponential decays of appropriate correlation functions. Taking $\Theta(x) = \bar{\psi}(x)\Gamma\psi(x)$, where the choice of the matrix Γ in the spin and flavour space decides whether it is a π-meson correlator or a ρ-meson correlator, one can compute the correlation function $C(t)$ as

$$C(t) = \mathscr{Z}^{-1} \int \prod_{x,\hat{\mu}} \mathrm{d}U_x^\mu \prod_x \mathrm{d}\psi(x)\, \mathrm{d}\bar{\psi}(x) \prod_f \det M_f \mathrm{e}^{-S_G} \Theta(t)\Theta(0), \quad (5)$$

with $\Theta(t) = \sum_{\vec{x}} \Theta(\vec{x},t)$. As $t \to \infty$, $C(t) \simeq A\exp(-mt)$, yielding thus the lowest mass with quantum numbers of Θ. Its decay constant can be obtained from the coefficient A.

The Monte Carlo technique to evaluate $C(t)$, or the expectation value of any other observable, consists of (1) generating a set of links $\{U_x^\mu\}$ for the whole lattice as large as possible, such that each set of $\{U_x^\mu\}$ occurs with a probability proportional to

$\prod_f \det M_f \cdot \exp[-S_G(\{U_x^\mu\})]$ and (2) evaluating $C(t)$ for each configuration $\{U_x^\mu\}$ and taking its average over all the configurations in the set.

A first hurdle in carrying out this program comes in the form of the fermion doubling problem. It turns out that a single flavour of quark on the lattice becomes equivalent to 16 $(= 2^d)$ flavours in the continuum limit, $a \to 0$, if one insists on having reasonable properties for S_F in eq. (1), such as (i) locality (discretizing the derivative using only few terms like two in eq. (1), (ii) chiral symmetry (γ_5 anticommutes with the lattice Dirac operator) and (iii) real Hamiltonian. The two popular solutions, which are used in the results presented below, are (i) Wilson fermions, which break *all* chiral symmetries on the lattice but have a one-to-one correspondence of flavours on the lattice and in the continuum and (ii) staggered or Kogut–Susskind fermions, which have an exact $U(1)$ chiral symmetry on the lattice but broken flavour symmetry. Furthermore, even the restored flavour symmetry in the $a \to 0$ limit for the latter is well-defined for four light flavours only. Recently, overlap fermions with exact chiral and flavour symmetry have also been used but these are computationally too difficult to handle. First results using them have provided resolution of an outstanding puzzle [1], details of which I will be unable to cover here. One hopes to have more and more interesting results from them soon.

The second hurdle relates to the enormity of the computational task if one wishes to generate the set of $\{U_x^\mu\}$ for full QCD, i.e., for a theory with all virtual quark loops included. Let us assume that the lattice has N_s sites in each of the space directions and N_t in time directions. Usually $N_\mathrm{t} \gg N_\mathrm{s}$ for a zero temperature propagator calculation, while $N_\mathrm{t} \ll N_\mathrm{s}$ for a finite temperature calculation. The temperature $T = 1/(N_\mathrm{t} a)$ and the spatial volume of the lattice $V = L^3 = N_\mathrm{s}^3 a^3$. The continuum limit corresponds to making the lattice finer by reducing a, and thus correspondingly making the lattice size $N_\mathrm{s}^3 \times N_\mathrm{t}$ bigger so that T and L are held constant in physical units. The current best algorithm, called the HMC algorithm, to generate a configuration of $\{U_x^\mu\}$ for full QCD needs computer time which scales as $V^{5/4}$ and $(m_q^{\mathrm{sea}} \cdot a)^{-5/2}$. Thus it increases rapidly as the sea quark mass is lowered and/or continuum limit is approached. The possible solutions, in increasing order of severity of approximations but decreasing order of computer time, are (i) full QCD simulations on smaller lattices, (ii) partially quenched QCD simulations with am^{sea} large and greater than am^{valence} and (iii) quenched QCD simulations with $am^{\mathrm{sea}} = \infty$ (i.e. no dynamical quarks). The early lattice results and today's best results are obtained in the quenched approximation. Indeed, one has now begun to answer quantitatively the question as to how good the approximation itself is.

3. The phase diagram

The lines of phase transitions in the phase diagram for QCD are obtained by investigating the order parameters, the chiral condensate $\langle\bar{\psi}\psi\rangle$ and the average Polyakov loop. The former is a measure of the effective mass of quarks generated by interactions, whereas the latter, $\langle L\rangle$, with $L(\vec{x}) = \frac{1}{3}\prod_{t=1}^{N_\mathrm{t}} \mathrm{tr}\, U_4(\vec{x},t)$, is thought to be a measure of the free energy of a static quark. Varying the coupling $\beta = 6/g^2$ in eqs (3) and (4), one varies the lattice spacing, and thus the temperature. From the temperature dependence of the order parameters, one can infer about the nature and the location of the phase transition, if any. These depend on the number of light flavours. Theoretical expectations based on effective models exploiting only the symmetries of the Lagrangian have lead to a phase diagram depicted in the left panel of figure 1. Varying the quark masses along its axes one goes

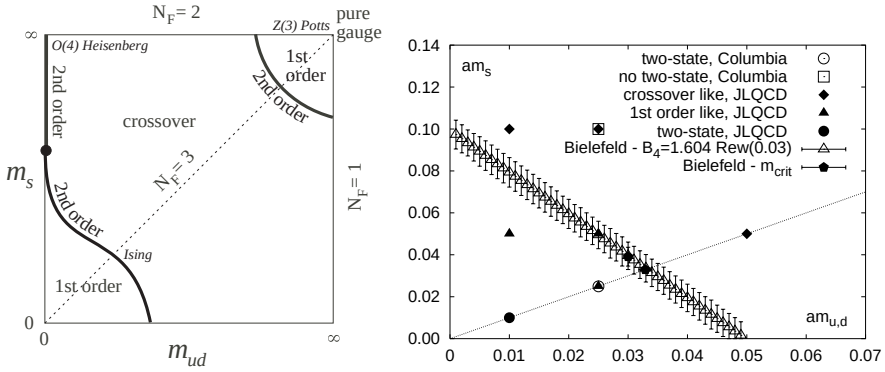

Figure 1. Theoretical expectations and simulation results for QCD phase diagram.

over to different number of flavours. As seen in figure 1, the chiral phase transition for two massless flavours is expected to be of second order while for massless three flavours, it is first. Consequently, finite masses should weaken (wash out) the transition for $N_f = 3(2)$. A lot of work has been done over the past years to explore this phase diagram numerically. The good news from these results (on small N_t lattices) so far is:

- Transition temperature for two light dynamical quarks agree for Wilson quarks (171(4) MeV [2]) and staggered quarks (173(8) MeV [3]).
- Transition seems to be continuous in both cases.
- Transition temperature for three light flavours: 154 ± 8 MeV [3].
- Theoretical expectations on the phase diagram, shown in figure 1 (left panel), work out too. This is seen in the right panel which shows simulation results on the lower left corner of the expected phase diagram. Taken from [4], it shows the results of the Bielefeld group with those of Columbia and JLQCD and emphasizes this agreement with the theoretical expectations.

The bad news, however, is that the critical exponents do not match for the two types of quarks: one obtains $O(4)$-like exponents for only Wilson quarks whereas no stable exponents seem to emerge from the staggered quark simulations. Thus the order of the phase transition is *not* yet established firmly. The possible causes of this crucial discrepancy could be (i) the fermion symmetry problem, (ii) too small lattices etc. One may wonder what effect the realistic $m_u \neq m_d$ may have on the above. Recent results [5] show that for $1 \leq m_d/m_u \leq 2$, the transition stays put. Figure 2 displays the order parameters on an $8^3 \times 4$ lattice for simulations with $m_d/m_u = 1$ (dashed), 2 (full) and 10 (dotted). The nature of the curves seems to remain roughly the same, with a significant shift in the location of transition only for $m_d/m_u = 10$.

3.1 *Non-zero baryonic density ($\mu_B \neq 0$)*

Lattice QCD at non-zero baryon density may help us in understanding, or even deriving, an interesting physical phenomena, namely, colour superconductivity, which may find applications in the astrophysics of strange quark stars. From a theoretical viewpoint, it is, of

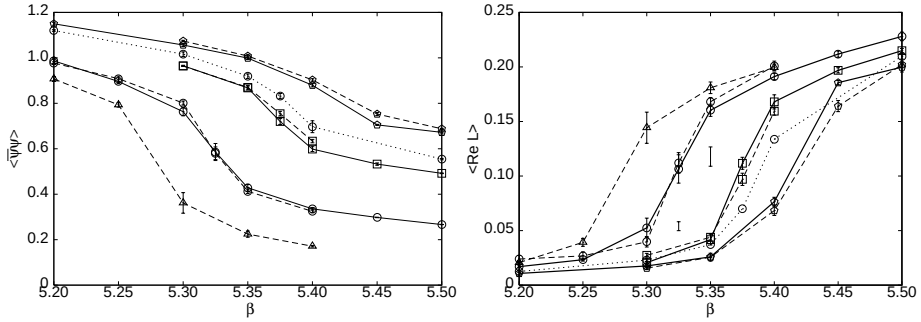

Figure 2. Effect of isospin breaking on the order parameters $\langle\bar{\psi}\psi\rangle$ and $\langle L\rangle$.

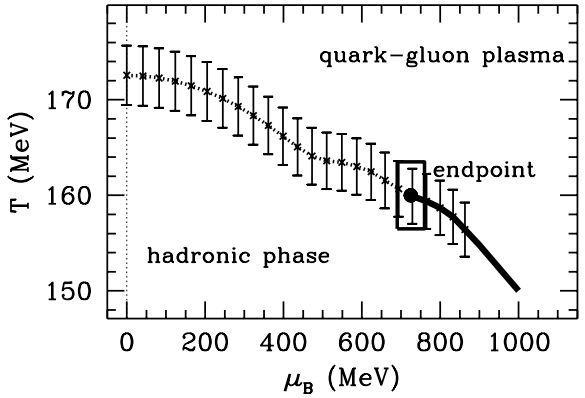

Figure 3. $\mu_{\rm B}$–T phase diagram for QCD.

course, crucial in completing the $\mu_{\rm B}$–T phase diagram of QCD. Both the numerical and the analytical methods used at finite temperature are inadequate in this case due to the fact that the fermionic determinant det $M(\mu)$ is complex for $\mu \neq 0$, commonly referred to as the sign (or the phase) problem. There have been some new exciting developments in the recent past for small μ. Most earlier attempts comprised of exploring first the zero temperature axis, where the problem is hardest. Recognizing this, the latest strategy has been to work for small μ in the vicinity of the quark–hadron transition, and study its behaviour as μ is turned on. Various methods [6], such as the re-weighting method, a Taylor expansion in μ, analytic continuation from imaginary μ, have lead to similar results, shown in figure 3 for the re-weighting method.

Using small $N_{\rm s}^3 \times 4$ lattices, with $N_{\rm s} = 4, 6, 8$ and somewhat heavy u, d quarks, a critical end-point was found at $T = 160(4)$ MeV, $\mu = 725(35)$ MeV. Increasing μ further led to a first-order phase transition line shown by the thick line in figure 3. Note the very mild temperature dependence in figure 3. A simple extrapolation to $T = 0$ suggests a huge value for the critical μ there which is in sharp contrast with various naive models and expectations unless the transition line exhibits a sharp bend at higher μ. One hopes to see in future results for larger $N_{\rm t}$ and thus free of lattice artifacts. Another interesting issue for RHIC physics may be the possible shift of the end-point as m_{ud} is decreased to realistic values.

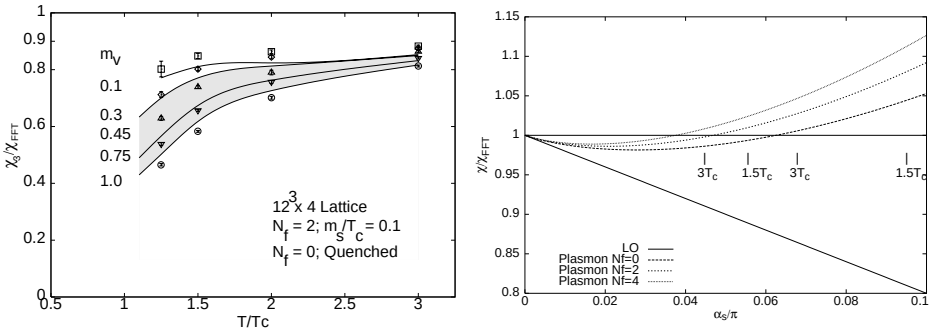

Figure 4. Quark number susceptibility from numerical simulations (left) and perturbation theory (right).

The Taylor expansion method needs quark number susceptibilities explicitly which is the subject of our next section in view of its independent physical and theoretical relevance.

4. Quark number susceptibility

Quark number susceptibilities are crucial for some signatures of quark–gluon plasma such as fluctuations of charge and/or baryon number, and production of strangeness. Their additional theoretical importance is due to the check they provide on resummed perturbation expansions. Defining μ_f as the chemical potential for a flavour $f = u,d,s$ and $\mu_0 = \mu_u + \mu_d + \mu_s$ and $\mu_3 = \mu_u - \mu_d$ as baryon and isospin chemical potentials, the respective density and susceptibility can be obtained from eq. (4) as:

$$n_i = \frac{T}{V}\frac{\partial \ln \mathscr{Z}}{\partial \mu_i}, \quad \chi_{ij} = \frac{T}{V}\frac{\partial^2 \ln \mathscr{Z}}{\partial \mu_i \partial \mu_j}. \tag{6}$$

Setting $\mu_f = 0$ after taking the derivatives, $n_f = 0$ but χ_{ij} are non-trivial. The diagonal χs are found [7] to be

$$\chi_0 = \tfrac{1}{2}[\mathscr{O}_1(m_u) + \tfrac{1}{2}\mathscr{O}_2(m_u)], \tag{7}$$

$$\chi_3 = \tfrac{1}{2}\mathscr{O}_1(m_u), \tag{8}$$

$$\chi_s = \tfrac{1}{4}[\mathscr{O}_1(m_s) + \tfrac{1}{4}\mathscr{O}_2(m_s)]. \tag{9}$$

Here $\mathscr{O}_i$ are trace of products of M^{-1}, M' and M'' and are estimated by a stochastic method: $\mathrm{Tr}\, A = \sum_{i=1}^{N_v} R_i^\dagger A R_i / 2N_v$, and $(\mathrm{Tr}\, A)^2 = 2\sum_{i>j=1}^{L} (\mathrm{Tr}\, A)_i (\mathrm{Tr}\, A)_j / L(L-1)$, where R_i is a complex vector from a set of N_v, subdivided in L independent sets. Further details can be found in [7]. Earlier results concentrated on T close to T_c and fixed lattice quark mass ma. Recognizing their roles mentioned above, we simulated [7] both quenched and full QCD for fixed physical quark masses and at a much larger temperature range. Denoting by χ_{FFT} the ideal gas results for the same sized lattice, the ratio χ/χ_{FFT} is exhibited in figure 4. The data points show the results for valence quark masses between $0.1T_c$ and T_c for full QCD with two dynamical quarks of mass $0.1T_c$. The continuous curves are for quenched QCD

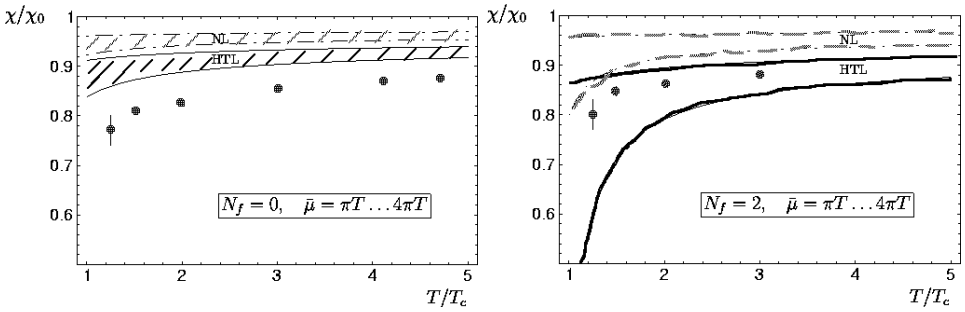

Figure 5. Comparison of lattice results with resummed, HTL and NL, perturbation theory for quenched QCD (left) and full QCD (right).

with the rest remaining the same. Using the range of strange quark mass from the particle data tables, one obtains $m_{\mathrm{u}}^{\mathrm{strange}}/T_{\mathrm{c}} \simeq 0.3$–$0.7$ ($N_f = 0$) and 0.45–1.0 ($N_f = 2$). The shaded region in figure 4 shows the range of strange quark susceptibility thus obtained. It is worth emphasizing here that the effect of removing the quenched approximation are at a level of few (~ 5) per cent although T_{c}, which sets the scale, differs by almost a factor two.

At sufficiently high temperatures, one can compute these susceptibilities from the usual weak coupling expansion which yields [8], $\chi/\chi_{\mathrm{FFT}} = 1 - 2(\alpha_{\mathrm{s}}/\pi) + 8\sqrt{(1+0.167N_f)}(\alpha_{\mathrm{s}}/\pi)^{3/2}$. This leads to the predictions that (i) its minimum value is 0.981(0.986) at a coupling $\alpha_{\mathrm{s}} = 0.03(0.02)$ for $N_f = 0(2)$ and (ii) in the range $1.5 \leq T/T_{\mathrm{c}} \leq 3$ the susceptibility is 0.99–0.98 (1.08–1.03) for $N_f = 0(2)$. The latter seems to be at odd with the Monte Carlo results both qualitatively and quantitatively as can be seen in figure 4. Indeed the temperatures where the minimum is reached are also much higher than $3T_{\mathrm{c}}$ and thus inaccessible to even the planned future heavy ion experiments.

The discrepancy with the straightforward perturbation theory is similar to what was found in other thermodynamical quantities such as the pressure or entropy. Various schemes to resum the perturbation series have been advocated in those cases to explain the lattice results. The results above for susceptibilities provide a good testing ground for these schemes, since a good scheme should predict the removal of the discrepancy above.

Figure 5 compares the simulation results with two, the HTL and the improved NL schemes, details of which can be found in [9]. One sees that the discrepancy still persists for the more precise quenched QCD results (left panel). One possible explanation is, of course, that our results for $N_{\mathrm{t}} = 4$ have strong lattice artifacts. We therefore went ahead to check them for larger N_{t} and improved actions. Another even more glaring discrepancy was found in our results for the off-diagonal susceptibility, χ_{ud}. It was seen in the simulations to be compatible with zero within $1/\sigma \sim O(10^{-6})$ for $T > T_{\mathrm{c}}$. It is identically zero for an ideal gas but $O(\alpha_{\mathrm{s}}^3)$ in perturbation theory, and is thus expected to be two orders larger: $\chi_{ud} \sim O(10^{-4})$!!

In a recent work [10], we attempted the task of taking the continuum limit by investigating larger N_{t}: 6, 8, 10, 12 and 14 and by employing the Naik action. It is improved by $O(a)$ compared to the staggered action. Introduction of μ is non-trivial for it but can be done [11].

The left panel of figure 6 displays the improvement due to the change of action for ideal quark gas. The continuum limit $a \to 0$, which at fixed temperature is equivalent to

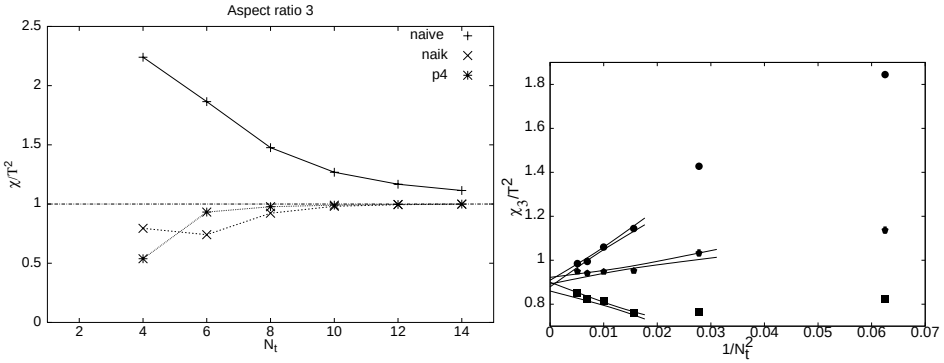

Figure 6. Comparison of ideal gas results for different fermion actions (left) and extrapolation of results for quenched QCD at $2T_c$ (right).

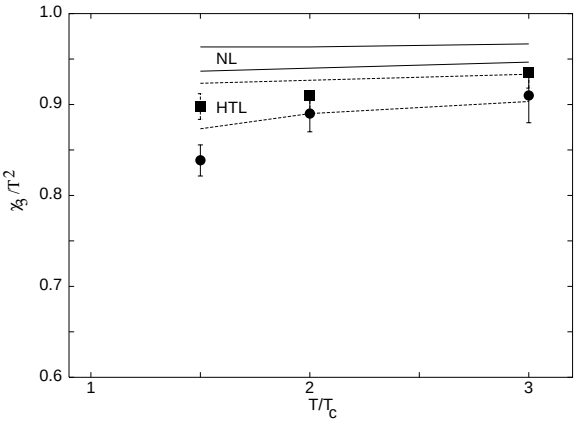

Figure 7. Quark number susceptibility in continuum quenched QCD as a function of T/T_c for the Naik action (squares) and staggered action (circles).

taking $N_t \to \infty$, is approached much faster for the improved action, thus permitting one to use smaller lattices for the latter. Note, however, that discretization errors are present in *all* cases, and thus extrapolation is required for each of them. The advantage of the improved action is in a smoother limiting function for smaller N_t. The right panel shows the extrapolation of quenched QCD results for quark number susceptibility at $2T_c$ for the staggered (top set) and Naik action (middle set). In the former case, extrapolation for $\chi/\chi_{\rm FFT}$ (bottom set) is also shown. The unique limit in all cases within errors is a signal of the result being the true continuum limit. Both fermion actions lead to an $N_t^{-2} \sim a^2$ behaviour, which is a lot milder for the Naik fermions.

Carrying out this process at other temperatures as well, the continuum susceptibility can be extracted as a function of T. The results of [10] for it in the quenched approximation are displayed in figure 7 along with the HTL and NL perturbation theory results. A broad agreement is seen within the errors although the leading order (HTL) results seem to be in better agreement than the next-to-leading order (NL), which is somewhat counter-intuitive.

From these continuum results one can extract many quantities of interest for heavy-ion collisions. The primary amongst them is the Wroblewski parameter. Defined as the ratio of the strange particles and the non-strange particles produced in a collision, it has been studied widely as a measure of the strangeness production. Interestingly, most heavy-ion collision data seems to yield a factor two higher value for it than other hadronic collisions. Using the quark number susceptibilities, and under certain assumptions [12], one can obtain $\lambda_s(T_c) = 2\chi_s/(\chi_u + \chi_d) \approx 0.4$–$0.5$ [10] which compares remarkably well with its latest RHIC value 0.47 ± 0.4. While the puzzle of the lattice results with respect to the resummed perturbation theory, seen in figure 5, got resolved significantly by going to the limit of vanishing lattice spacing, seen in figure 7, the huge discrepancy for χ_{ud} seems to persist even in that limit. In particular, it behaves the same way for *all* N_t and both fermions, leading to the same $O(10^{-6})$ values in continuum too. Solving this mystery would enhance our understanding of the plasma phase further.

5. Screening lengths

A possible explanation for the discrepancies discussed in the previous section is the role of non-perturbative physics which may be seen in various screening lengths. These are obtained from the exponential decay of the correlation functions in a manner analogous to the statistical mechanics. For an operator $\bar{\psi}\Gamma\psi$ created at origin and destroyed at (x,y,z,t), the correlation function in terms of the quark propagator with the source at origin, $M^{-1}(x,y,z,t;0,0,0,0)$, is:

$$C_\Gamma(z) = \sum_{x,y,t} \langle M^{-1}_{\alpha\beta}(x,y,z,t;0,0,0,0)\Gamma M^{\dagger -1}_{\beta\alpha}(0,0,0,0;x,y,z,t)\Gamma\rangle. \tag{10}$$

Here Γ stands for the spin-flavour matrix depending upon the quantum number of the mesonic channel and α, β are colour indices. From previous investigations [13] of the screening lengths it is known that the quark–gluon phase above T_c has chiral symmetry restored with parity partners being degenerate. Moreover, all the screening lengths except that for pion (and its scalar partner) are found to be close to their free field values. These results lead to scenarios of interacting pions in the quark–gluon phase. Figure 8 has in its left panel the behaviour of χ_3/T^2 (open symbols) and $\chi_\pi/10T^2$ (filled) as a function of the pion screening length. The latter was obtained [7] by summing its correlation function defined above over the entire lattice. The simulations were done on $N_t = 4$ lattices with $N_z = 16$ at $2T_c$ (lower set) and $3T_c$. Their similar behaviour suggests that both could have perhaps the same non-perturbative effect. This is understood easily when one notes that χ_3 is also a sum of a propagator of non-local vector meson.

Taking continuum limit is therefore again interesting in view of the change seen in χ_3 in this limit. Indeed, the right panel of figure 8 demonstrates that on finer lattices, $a = 1/8T - 1/12T$, even the pion screening length becomes degenerate with those of ρ, i.e., is also close to the corresponding FFT value! These results were obtained on lattices up to 48×26^2 at $2T_c$ using a quark mass $m_v/T_c = 0.03$. Does it then imply the absence of any non-perturbative physics? In order to answer that, one needs to note that the chiral condensate, $\langle\bar{\psi}\psi\rangle$ differs from FFT by 2, as do the detailed shapes of the correlators. Figure 9 displays the results for the pseudoscalar (circles) and vector correlators (pluses) along with the corresponding free field results (bold continuous lines). It may be noted

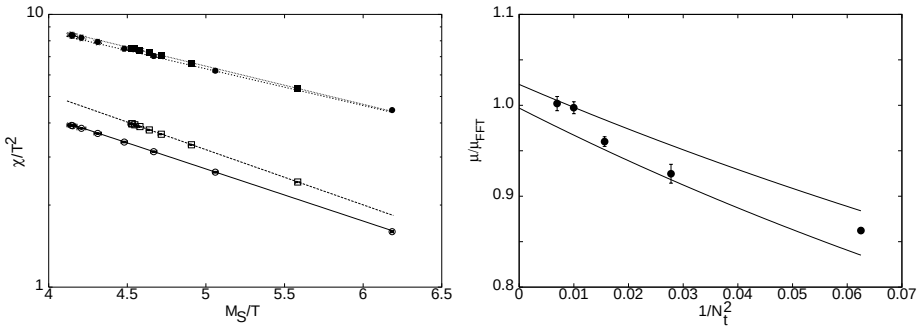

Figure 8. Quark number and pion susceptibility as a function of m_π/T_c (left) and continuum limit of the pion screening length (right).

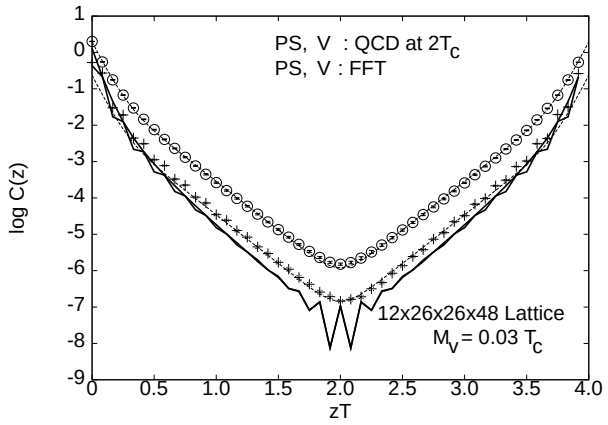

Figure 9. Pseudoscalar (circles) and vector correlators (pluses) along with the corresponding free field results (bold lines).

that the *same* fit with only changed normalization is shown for both sets of data. Thus, the (leading) screening lengths in both channels are seen to be close to each other.

6. Summary

One of the major developments of the recent past in lattice QCD is the firming up of the QCD phase diagram in μ–T plane on small N_t. Different fermions (staggered and Wilson), different methods of simulations for non-zero μ, all lead to good agreement on the qualitative as well as the quantitative aspects. All estimates of T_c, and (T_E, μ_E) are mutually consistent.

Various physical quantities have been obtained in the continuum limit in the quenched approximation to QCD. These include the quark number susceptibilities which are directly relevant to the physics of quark–gluon plasma signals at RHIC. The quenched lattice QCD estimate of Wroblewski parameter, λ_s, which is a measure of strangeness production in heavy-ion collision experiments, is in excellent agreement with the RHIC and SPS results.

The susceptibilities also provide a test-bed for resummations of perturbation series. The continuum results in quenched QCD show that there is scope for improvement in the resummation schemes. The pion screening length approaches its free field value, and is close to that for ρ, in the continuum limit of $N_t \to \infty$ for quenched QCD.

Many questions still remain for full QCD with two light and one moderately heavy quark corresponding to real world. The order of the transition, continuum limit of physical quantities etc. are all awaiting to be resolved and settled.

References

[1] R V Gavai, S Gupta and R Lacaze, *Phys. Rev.* **D65**, 094504 (2002)
[2] A Ali Khan *et al*, *Phys. Rev.* **D63**, 034502 (2001)
[3] F Karsch, E Laermann and A Peikert, *Nucl. Phys.* **B605**, 579 (2001)
[4] Ch Schmidt *et al*, hep-lat/0209009
[5] R V Gavai and S Gupta, *Phys. Rev.* **D66**, 094510 (2002)
[6] Z Fodor and S D Katz, *J. High Energy Phys.* **0203**, 014 (2002)
C R Allton *et al*, *Phys. Rev.* **D66**, 074507 (2002)
Ph de Forcrand and O Philipsen, *Nucl. Phys.* **B642**, 290 (2002)
M D'Elia and M P Lombardo, hep-lat/0205022
[7] R V Gavai and S Gupta, *Phys. Rev.* **D64**, 074506 (2001)
R V Gavai, S Gupta and P Majumdar, *Phys. Rev.* **D65**, 054506 (2002)
[8] J I Kapusta, *Finite-temperature field theory* (Cambridge University Press, Cambridge, UK, 1989)
[9] J-P Blaizot, E Iancu and A Rebhan, *Phys. Lett.* **B523**, 143 (2001)
P Chakraborty, M G Mustafa and M H Thoma, *Euro. Phys. J.* **C23**, 591 (2002)
[10] R V Gavai and S Gupta, *Phys. Rev. D* (in press); hep-lat/0211015
[11] S Naik, *Nucl. Phys.* **B316**, 238 (1989)
R V Gavai, hep-lat/0209008
[12] R V Gavai and S Gupta, *Phys. Rev.* **D65**, 094515 (2002)
[13] C Detar and J B Kogut, *Phys. Rev. Lett.* **59**, 399 (1987)
S Gottlieb *et al*, *Phys. Rev. Lett.* **59**, 1881 (1987)
K D Born *et al*, *Phys. Rev. Lett.* **67**, 302 (1991)